



Article

Study on Structural Evolution, Thermochemistry and Electron Affinity of Neutral, Mono- and Di-Anionic Zirconium-Doped Silicon Clusters $ZrSi_n^{0/-/2-}$ ($n = 6-16$)

Caixia Dong^{1,2}, Limin Han¹, Jucai Yang^{1,3,*} and Lin Cheng^{1,*} 

¹ Inner Mongolia Key Laboratory of Theoretical and Computational Chemistry Simulation, School of Chemical Engineering, Inner Mongolia University of Technology, Hohhot 010051, China; Dongcx201011@163.com (C.D.); hanlimin@imut.edu.cn (L.H.)

² School of Mining and Technology, Inner Mongolia University of Technology, Hohhot 010051, China

³ School of Energy and Power Engineering, Inner Mongolia University of Technology, Hohhot 010051, China

* Correspondence: yangjc@imut.edu.cn (J.Y.); lcheng1983@aliyun.com (L.C.); Tel.: +86-0471-657-6145 (J.Y.)

Received: 14 May 2019; Accepted: 8 June 2019; Published: 15 June 2019



Abstract: We have carried out a global search of systematic isomers for the lowest energy of neutral and Zintl anionic Zr-doped Si clusters $ZrSi_n^{0/-/2-}$ ($n = 6-16$) by employing the ABCluster global search method combined with the mPW2PLYP double-hybrid density functional. In terms of the evaluated energies, adiabatic electron affinities, vertical detachment energies, and agreement between simulated and experimental photoelectron spectroscopy, the true global minimal structures are confirmed. The results reveal that structural evolution patterns for neutral $ZrSi_n$ clusters prefer the attaching type ($n = 6-9$) to the half-cage motif ($n = 10-13$), and finally to a Zr-encapsulated configuration with a Zr atom centered in a Si cage ($n = 14-16$). For Zintl mono- and di-anionic $ZrSi_n^{-/2-}$, their growth patterns adopt the attaching configuration ($n = 6-11$) to encapsulated shape ($n = 12-16$). The further analyses of stability and chemical bonding make it known that two extra electrons not only perfect the structure of $ZrSi_{15}$ but also improve its chemical and thermodynamic stability, making it the most suitable building block for novel multi-functional nanomaterials.

Keywords: the most stable neutral and Zintl anionic Zr-doped silicon clusters; structural evolution patterns; simulated photoelectron spectroscopy; stability; HOMO-LUMO gap

1. Introduction

Transition metal (TM) silicides as novel functional materials have been extensively utilized in diverse fields such as aerospace, microelectronic device manufacturing, optical instruments, magnetic material, and the chemical industry because of their oxidation resistance, high-temperature stability, and low electrical resistivity [1,2]. For example, in the early 1960s platinum silicide was successfully used to improve the rectifying characteristics of diodes [3]. Nickel silicide showed significantly enhanced catalytic activity in CO methanation [4]. Composite coatings including molybdenum silicide can be used for protection of missile nozzles and aero engine blades [5]. Zirconium silicide is an ideal device with significant potential applications as anode materials in Li-ion batteries, protective coating on zirconium-alloy fuel cladding in light water reactors, heating elements for electrical furnaces, and also can be incorporated into the semiconductor industry as large scale integrated circuits, Schottky barriers, Ohmic contacts, and rectifying contacts due to the fact that interfaces of zirconium and silicon have good lattice matching, sharp interfaces, low Schottky barrier heights, high conductivity, and excellent thermal stability [1,2,6-8]. Therefore, a large amount of research on zirconium silicides

was carried out in the past few decades. These investigations concentrate primarily on the formation of amorphous zirconium silicides and have suggested that nanoscales such as nanoclusters, nanotubes, and ultrathin films play a pivotal role in such physical and chemical processes. On the other hand, the miniaturization of devices approaching the sub-nanometer regime could result in material with tunable electronic properties by altering size, shape, and composition based on the application, but it would require a detailed understanding of the interplay between individual transition metals and silicon atoms. Accordingly, it is very significant to explore the evolution of zirconium silicide nanoclusters in the transition from the molecular to the condensed phase.

There have been some previous investigations on Zr-doped silicon clusters. Stimulated by the first observation of TM@Si_n ($\text{TM} = \text{Cr, Mo, W}$, $n = 15$ and 16) compounds formed by the laser vaporization supersonic jet expansion technique, the characters of the middle-sized Zr-encapsulated Si clusters were executed theoretically [9]. Kumar et al. calculated the structural and electronic properties of Zr@Si_n ($n = 8\text{--}20$) by using the ab initio pseudopotential plane wave method and density functional theory (DFT) with B3PW91 and PW91PW91 schemes and concluded that the evolution pattern of the ground state structure was basketlike open structures for $n = 8\text{--}12$, while for $n = 13\text{--}16$, it was Zr-encapsulated Si clusters; and for larger-size $n = 17\text{--}20$, it was capped Zr@Si_{16} cages [10–15]. Sen and Mitas reported on a theoretical study of the electronic structure of clusters with an encapsulated TM atom (TM atom from 3d, 4d, and 5d series) in a Si_{12} hexagonal prism (HP) cage [16]. Lu and Nagase investigated structural and electronic properties of TMSi_n ($\text{TM} = \text{W, Zr, Os, Pt, Co, etc.}$) in a range of $8 \leq n \leq 20$ by using B3LYP with LanL2DZ basis sets for the TM atom and the LanL2DZ(d) basis set for Si atoms, and found that the ground state structure of Zr@Si_{14} was a distorted HP with Si_2 decorating the lateral prism faces, and it was 0.16 eV lower in energy than the distorted HP with two Si atoms symmetrically capping the lateral prism faces [17]. Subsequently, Han and co-workers investigated systematically the total energies, equilibrium geometries, growth pattern mechanisms, and natural population analysis (NPA) of ZrSi_n ($n = 1\text{--}16$) by using B3LYP with LanL2DZ basis sets, and proposed that when $n \leq 7$, the ground state ZrSi_n structures, excluding ZrSi_3 , maintain the same framework as Si_{n+1} , but when $n = 8\text{--}16$, the Zr atom evidently disturbs the geometries of the Si clusters, and its localized position gradually changes from the surface site to the concave site of the open Si cage and to the encapsulated site of the sealed Si cage [18]. Wu et al. studied the bond distances, vibrational frequencies, adiabatic electron affinities (AEAs), ionization potential, and dissociation energies of TMSi ($\text{TM} = 3\text{d, 4d, 5d}$ elements) and their charged ions by using the B3LYP scheme [19]. Furthermore, the geometries and electronic properties of Zr₂-doped silicon clusters were reported [20,21]. On the experimental aspect, Koyasu et al. investigated the equilibrium configurations, electronic structures, and properties of MSi_n ($\text{M} = \text{Zr, Sc, Y, Lu, Ti, Hf, V, Nb, and Ta}$, $n = 6\text{--}20$) by means of anion photoelectron spectroscopy (PES) and their reactivity to H_2O adsorption, presented their AEAs and vertical detachment energies (VDEs), and discussed the cooperative effect between their geometric and electronic structures [22,23]. Recently, bond dissociation energies, valence orbitals, AEAs, and VDEs of ZrSi have been measured by using resonant two-photon ionization spectra and photoelectron imaging spectroscopy, respectively [1,24,25].

Although these theoretical investigations focused on the structural stability and evolution of Zr-doped neutral Si_n ($n \leq 16$) clusters and offered significant information for further theoretical and experimental research, a few problems still exist in Zr-doped Si_n species. First, as Maroulis et al. pointed out, the dependence of the predicted ground state structure and property on adopted computational methods and basis sets exists especially for clusters including TM atoms with a partially filled *d* sub-shell [26,27]. The performance of double hybrid (DH) DFT is better than that of pure or single hybrid DFT [28,29]. Considering the sensitivity of basis sets, we choose all-electron basis sets of triple-zeta quality (cc-pVTZ) for Si atoms and ECP28MDF-VDZ (cc-pVDZ-PP) basis sets for Zr atoms. Second, losing the ground state geometry is probable in the period of the initial isomer choice without a global search scheme [30–32]. Third, the global minimum is generally verified by comparison of the theoretical and experimental data in detail, owing to the fact that up to now there is no experimental equipment for directly surveying the lowest energy structure of clusters. Fourth, accurate theoretical

investigations of neutral and anionic Zr-doped silicon clusters are deficient, especially for the important Zintl anions ZrSi_n^{2-} . As a matter of fact, only by understanding the ground state structure and the growth pattern of Zr-doped Si clusters can we explain the diversity of their properties. Herein, the unbiased ABCluster global search technique coupled with the mPW2PLYP method and the cc-pVTZ basis set for Si atoms and the cc-pVDZ-PP basis set for Zr atoms is utilized for the configuration optimization of neutral and Zintl anionic $\text{ZrSi}_n^{0/-2-}$ ($n = 6-16$) with the objective of systematically investigating their structural stability and growth patterns, accurately probing the thermochemistry and electron affinity, illuminating details of the bonding characteristic, and offering significant data for further theoretical and experimental investigations of silicon clusters doped with other TM atoms.

2. Results and Discussion

2.1. Evolution of the Ground State Structure

The global minimal structures and/or competing global minimal isomers optimized with the mPW2PLYP/MIDDLE method for neutral, mono-, and di-anionic $\text{ZrSi}_n^{0/-2-}$ species are illustrated in Figures 1–3, respectively. The corresponding low-lying geometries are illustrated in Figures S1–S3 in Supplementary Information, respectively, where the relative energies from the lowest energy structure calculated at the mPW2PLYP/LARGE//mPW2PLYP/MIDDLE level and point group are also given. Conformational population (%) for low-lying geometries of $\text{ZrSi}_n^{0/-2-}$ species are listed in Table S1. The average binding energy (E_b), electronic state, and NPA charge on Zr atoms for the global minimum are provided in Table 1.

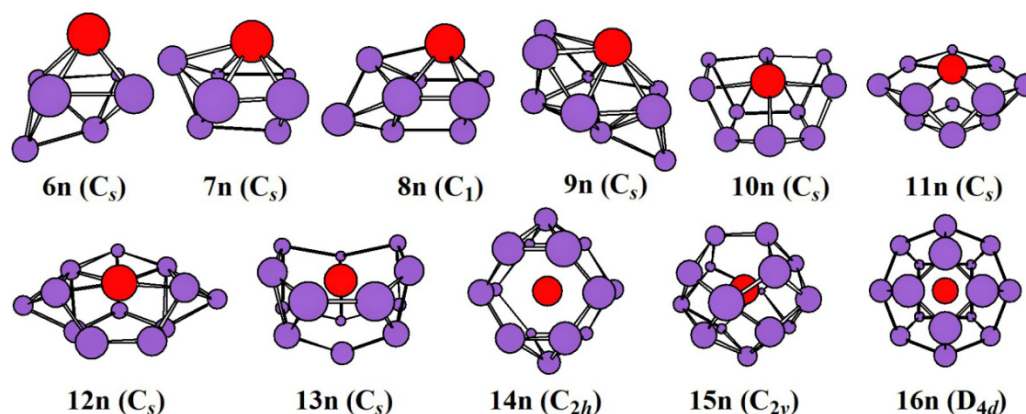


Figure 1. The lowest-energy structures of ZrSi_n ($n = 6-16$) and their point group.

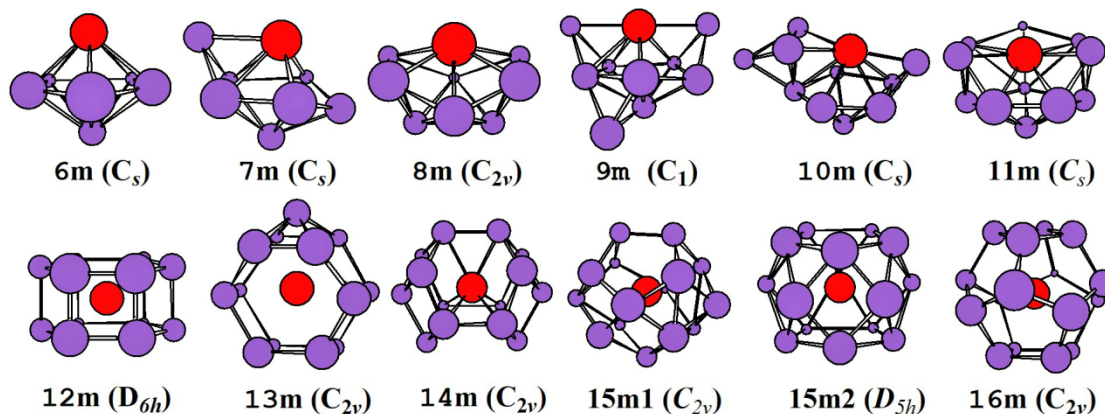


Figure 2. The lowest-energy structures of mono-anionic ZrSi_n^- ($n = 6-16$) and their point group.

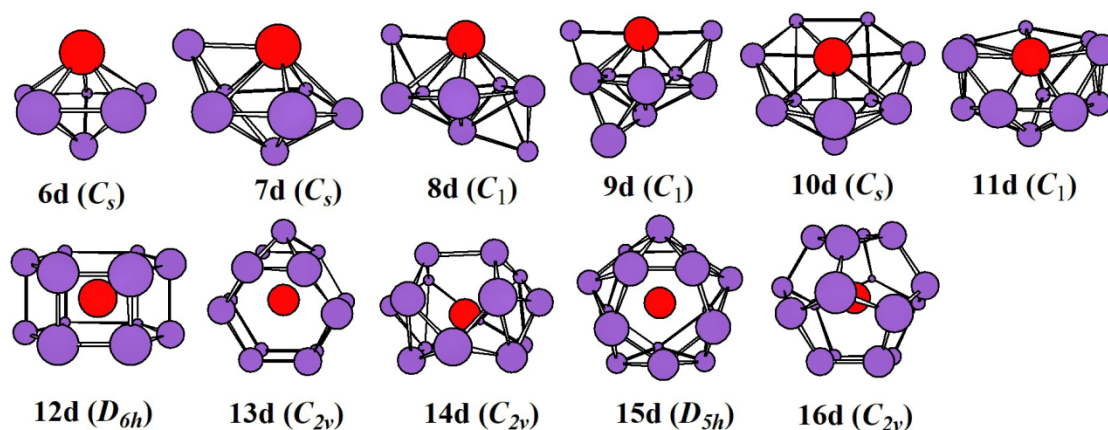


Figure 3. The lowest-energy structures of di-anionic $ZrSi_n^{2-}$ ($n = 6-16$) and their point group.

Table 1. Electronic state, average bonding energy E_b (eV), and the charge on the Zr atom $Q(Zr)$ (a.u.) of the ground state structure of $ZrSi_n^{0/-2-}$ ($n = 6-16$) clusters.

n	$ZrSi_n$				$ZrSi_n^-$			$ZrSi_n^{2-}$		
	State	E_b	$Q(Zr)$	State	E_b	$Q(Zr)$	State	E_b	$Q(Zr)$	
6	1A_1	3.44	-0.13	$^2A''$	3.57	0.25	$^1A'$	3.95	-0.49	
7	$^1A'$	3.51	-0.34	$^2A'$	3.63	0.04	$^1A'$	4.02	-0.58	
8	1A	3.57	-0.16	2B_2	3.68	-0.40	1A	4.02	-0.31	
9	1A_1	3.59	-0.50	2A	3.7	-0.20	2A	4.02	-0.70	
10	$^1A'$	3.59	-0.53	$^2A'$	3.71	-0.40	$^1A'$	4.09	-0.90	
11	$^1A'$	3.63	-0.98	$^2A''$	3.75	-0.60	1A	4.08	-0.76	
12	$^1A'$	3.67	-0.87	$^2A_{2u}$	3.76	-1.20	$^1A_{1g}$	4.12	-1.33	
13	$^1A'$	3.67	-1.87	2A_1	3.81	-1.20	1A_1	4.12	-1.24	
14	1A_g	3.72	-2.66	2B_1	3.83	-1.20	1A_1	4.13	-1.45	
15	1A_1	3.76	-3.31	$^2A_1'$	3.85	-1.29	$^1A_1'$	4.16	-2.90	
16	1A_1	3.83	-1.89	2B_1	3.91	-0.90	1A_1	4.13	-0.77	

The ground state of all neutral $ZrSi_n$ ($n = 6-16$) is predicted to be a singlet. The growth pattern adopts the attaching type to the half-cage motif, and finally to the Zr-encapsulated configuration with the Zr atom centered in a Si cage. The global minimum is a face-capped tetragonal bipyramid for $ZrSi_6$. For $n = 7-9$, their ground state structure can be viewed as attaching one, two, and three Si atoms to the face of the $ZrSi_6^-$ cluster, respectively. For $n = 10-13$, they are half-cage motifs consisting of two five-membered rings, a seven-membered and four-membered ring, a seven-membered and five-membered ring, and a seven-membered and six-membered ring, respectively. For $n = 14-16$, their ground state structures are encapsulated configurations with the Zr atom located in the Si cage. The cage of $ZrSi_{14}$ is a distorted HP with two Si atoms symmetrically capping the lateral prism faces. The cage comprised of two pentagons and ten quadrilaterals (TPTQ) is predicted to be the global minimum for $ZrSi_{15}$. A fullerene cage is calculated to be the ground state structure for $ZrSi_{16}$. It is noted that the ground state structures for $n = 7-15$ presented herein are different from those reported in [18]. In addition, the most stable structures for $n = 8-13$ differ from those presented in [14], and for $n = 14$ differs from those presented in [15,17].

The ground state for all mono-anionic $ZrSi_n^-$ ($n = 6-16$) is calculated to be a doublet. Their structural growth pattern prefers the attaching type to the encapsulated shape with the Zr atom centered in the Si cage. The global minimum of $ZrSi_6^-$ is a distorted pentagonal bipyramid with the Zr atom on the principal axis. For $n = 7-11$, their ground state structures can be regarded as attaching one, two, three, four, and five Si atoms to the face of the $ZrSi_6^-$ cluster, respectively. That is, the distorted pentagonal bipyramid of $ZrSi_6^-$ is the basic structural unit for $n = 6-11$. For $n = 12-16$, their global minima are encapsulated shapes with the Zr atom residing in the Si cage. The HP, capped HP, THSQ

(three hexagon and six quadrangle), and fullerene cages are evaluated to be the most stable structures of ZrSi_{12}^- , ZrSi_{13}^- , ZrSi_{14}^- , and ZrSi_{16}^- , respectively. For ZrSi_{15}^- , the TPTQ (15m1) and five-capped PH (pentagonal prism) (15m2) are competitive for the global minimum due to the fact that they are degenerate in energy (the energy difference is only 0.01 eV). Although it is difficult to determine the ground state structure by energy in this situation, the 15m2 isomer is the most probable ground state structure based on simulated PES (see below). To our knowledge, only ZrSi_{16}^- was studied previously by Wu et al. [33].

The ground state structures for all di-anionic ZrSi_n^{2-} ($n = 6-16$) are evaluated to be singlet. The growth model of di-anionic ZrSi_n^{2-} species is consistent with that of mono-anionic clusters. For $n = 6-13, 15, 16$, the global minima of di-anionic ZrSi_n^{2-} are similar to those of their mono-anions. The cage of di-capped OHFP (one hexagon and four pentagon) is calculated to be the ground state structure for ZrSi_{14}^{2-} , which differs from that of the corresponding mono-anion.

The distribution of $\text{ZrSi}_n^{0/-2-}$ clusters at room-temperature by Boltzmann statistics can further support our results. From Table S1, we can see that the lowest-energy structures account for the largest proportion. This verifies the accuracy of the above ground state structures.

2.2. PES of Mono-Anionic Species

PES is one of the most important experimental tools to get insight into, and to extract electronic fingerprints from, a variety of atomic and molecular clusters as well as condensed-matter systems. Accordingly, the validity of the predicted ground state structures can be tested by way of comparing their theoretical and experimental PES spectra, in which two norms are used. One is the amount of distinct peaks and their position in the PES spectra, and another is the first VDE and/or AEA. The simulated PES of the global minimal structures coupled with the experimental PES spectra are pictured in Figure 4. The theoretical predicted AEAs and the first VDEs are provided in Table 2 along with experimental data. It can be seen from the simulated PES of ZrSi_6^- in the range of ≤ 5.8 eV that there are four distinct peaks (X, A–C) residing at 3.32, 3.63, 4.33, and 5.37 eV, of which the first three peaks are in excellent agreement with experimental data of 3.40, 3.60, and 4.30 eV [23]. The simulated PES of ZrSi_7^- has five different peaks (X, A–D) located at 2.86, 3.49, 4.16, 4.85, and 5.59 eV, of which the first three peaks are in excellent accord with the experimental values of 2.80, 3.20, and 4.00 eV [23]. For ZrSi_{12}^- and ZrSi_{16}^- , there are four discrete peaks (X, A–C) centered at 3.99, 4.30, 5.07, and 5.52 eV, and 2.65, 4.11, 4.70, and 5.61 eV, which reproduce well the experimental data of 4.10, 4.40, 4.90, and 5.50 eV, and 2.82, 4.30, 4.80, and 5.50 eV, respectively [22,23]. For ZrSi_{10}^- , four distinct peaks (X, A–C) residing at 3.35, 3.88, 4.45, and 5.58 eV are obtained. In addition to the first peak (X), the remaining three peaks (A–C) are very close to experimental data of 3.80, 4.90, and 5.60 eV, respectively [23]. For ZrSi_{14}^- , four peaks (X, A–C) centered at 3.18, 3.64, 4.59, and 5.16 eV are also obtained, but only later two peaks appear in the experimental PES and agree well with experimental data of 4.50 and 5.20 eV [23]. For $n = 8, 9, 11$, and 13, their simulated PES has many different peaks. The first 6–8 peaks reside at 2.81, 3.25, 3.84, 4.17, 4.59, and 5.39 eV, 2.76, 3.38, 3.83, 4.43, 4.72, 5.11, and 5.60 eV, 3.25, 3.43, 3.83, 4.27, 4.79, 5.02, 5.39, and 5.66 eV, and 3.53, 3.86, 4.43, 4.82, 5.09, and 5.76 eV, respectively. Unfortunately, only three peaks are observed in their experimental PES. And it seems experimentally that their first peaks are not observed analogous to ZrSi_{10}^- and ZrSi_{14}^- . For $n = 15$, the simulated PES of 15m1 and 15m2 isomers has four peaks (X, A–C) located at 3.00, 3.93, 4.40, and 4.96 eV, and 3.97, 4.51, 4.94, and 5.62 eV, respectively. Apart from first peak (X), the rest of peaks (A–C) for 15m2 are close to the experimental data of 4.70, 5.10, and 5.50 eV, respectively [23]. On the other hand, the three peaks of the experimental spectra of ZrSi_{15}^- are also simulated by the calculations with a shift of the first three peaks (X, A, and B) of the 15m2 isomer by 0.7 eV to the higher binding energy [23]. So we suggest that the 15m2 geometries are the most probable ground state structure. Comparing their theoretical and experimental AEAs (see Table 2), we can see that the AEAs of ZrSi_n^- ($n = 6-16$) excluding ZrSi_{11}^- , ZrSi_{12}^- , and ZrSi_{15}^- are agreement with those of experimental data. The mean absolute deviations from experimental values are 0.08 eV, and the largest errors are those of ZrSi_7^- and ZrSi_{13}^- which are off by 0.11 eV.

In short, good agreement between the theoretical and experimental PES spectra sheds further light on the validity of the predicted most stable structures. In light of our reliable theoretical predictions, we suggest that the experimental PES spectra of ZrSi_{11}^- and ZrSi_{15}^- species should be checked further. The cause lies in that their theoretical and experimental AEAs and VDEs have large differences.

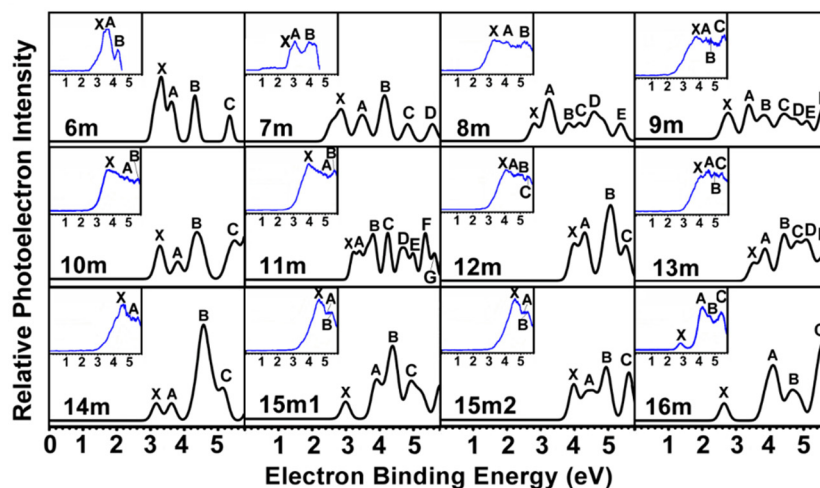


Figure 4. Photoelectron spectroscopy (PES) spectra of the most stable ZrSi_n^- ($n = 6-16$) clusters. The inserts show the experimental PES spectra taken from [22,23].

Table 2. Theoretical and experimental adiabatic electron affinity (AEA) and vertical detachment energy (VDE) for ZrSi_n^- ($n = 6-16$).

Species	AEA		VDE	
	Theor	Exptl	Theor	Exptl
6n←6m	2.24	2.30 ± 0.0043 ^a	3.32	3.4 ± 0.1 ^a
7n←7m	2.29	2.40 ± 0.0043 ^a	2.86	2.8 ± 0.1 ^a
8n←8m	2.31	2.30 ± 0.0043 ^a	2.81	3.3 ± 0.1 ^a
9n←9m	2.29	2.20 ± 0.0043 ^a	2.76	3.9 ± 0.1 ^a
10n←10m	2.64	2.70 ± 0.0043 ^a	3.35	3.8 ± 0.1 ^a
11n←11m	2.65	2.90 ± 0.0043 ^a	3.25	4.0 ± 0.1 ^a
12n←12m	2.50	2.90 ± 0.0043 ^a	3.99	4.1 ± 0.1 ^a
13n←13m	3.11	3.00 ± 0.0043 ^a	3.53	4.1 ± 0.1 ^a
14n←14m	2.90	3.00 ± 0.0043 ^a	3.18	4.5 ± 0.1 ^a
15n←15m1	2.87	3.20 ± 0.0043 ^a	3.00	4.7 ± 0.1 ^a
15n←15m2	2.86	3.20 ± 0.0043 ^a	3.97	4.7 ± 0.1 ^a
16n←16m	2.52	2.46 ± 0.080 ^b	2.65	2.9 ± 0.1 ^a

^a The data taken from [23]. ^b The data taken from [22].

2.3. Stability

The thermodynamic and chemical stability of the global minimal structures of $\text{ZrSi}_n^{0/-/2-}$ ($n = 6-16$) species are characterized by the E_b , second energy difference (Δ^2E) and the HOMO-LUMO (Highest Occupied Molecular Orbital - Lowest Unoccupied Molecular Orbital) energy gap (E_{gap}). The E_b and Δ^2E are calculated via the following expressions, where E is the total energy of the corresponding atom or cluster. The results are pictured in segments a and b of Figure 5, respectively.

$$E_b(\text{ZrSi}_n) = [E(\text{Zr}) + nE(\text{Si}) - E(\text{ZrSi}_n)] / (n + 1) \quad (1)$$

$$E_b(\text{ZrSi}_n^{-/2-}) = [E(\text{Zr}) + (n - 1)E(\text{Si}) + E(\text{Si}^{-/2-}) - E(\text{ZrSi}_n^{-/2-})] / (n + 1) \quad (2)$$

$$\Delta^2E(\text{ZrSi}_n^{0/-/2-}) = E(\text{ZrSi}_{n-1}^{0/-/2-}) + E(\text{ZrSi}_{n+1}^{0/-/2-}) - 2E(\text{ZrSi}_n^{0/-/2-}) \quad (3)$$

From Figure 5a we can see the data for E_b : di-anionic compounds > mono-anionic species > neutral clusters. The higher E_b , the more stable the relative stability. It is to say that Zintl anionic Zr-doped Si clusters are more stable than their neutral counterparts, particularly for di-anionic compounds. The cause lies in that neutral $ZrSi_n$ compounds still have a dangling bond. When they obtain electrons, these extra electrons decrease the dangling bonds and improve the stability; (Figure 5b) for neutral $ZrSi_n$ with $n = 9, 12,$ and $14,$ for mono-anionic $ZrSi_n^-$ with $n = 8, 11,$ and $13,$ and for Zintl di-anionic $ZrSi_n^{2-}$ with $n = 7, 10, 12$ and $15,$ the compounds are more stable than their neighbors. These results are obviously reproduced in Figure 5b because the Δ^2E is a sensitive estimate for relative stability.

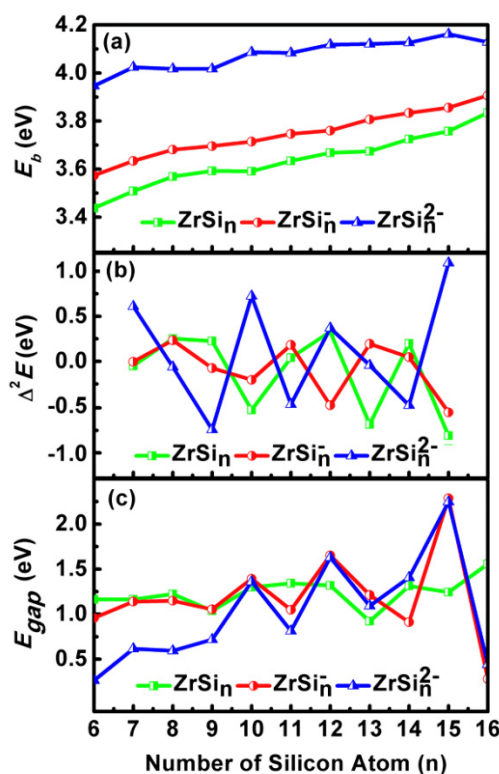


Figure 5. Size dependences of (a) average bonding energy (E_b), (b) second energy difference (Δ^2E), and (c) HOMO-LUMO energy gap (E_{gap}) for the ground state $ZrSi_n^{0/-/2-}$ ($n = 6-16$) clusters.

E_{gap} as a significant physical parameter can be regarded as an index of chemical reactivity, particularly for photochemical reactivity. Larger values of the E_{gap} stand for weaker chemical reactivity. Baerends et al. found that the E_{gap} predicted by pure DFT is closer to the real optical gap than that calculated by hybrid DFT [34]. In light of this finding, the PBE E_{gap} of $ZrSi_n^{0/-/2-}$ ($n = 6-16$) compounds are pictured in Figure 5c as functions of the size of Si clusters, and mPW2PLYP E_{gap} is pictured in Figure S4 in Supplementary Information. It can be seen from Figure S4 that the E_{gap} of mPW2PLYP is larger than that of PBE by 2.46 eV. The E_{gap} of PBE is a very good approximation to the optical gap. The PBE E_{gap} of 1.56 eV for $ZrSi_{16}$ is in good agreement with an approximate experimental value of 1.36 eV [22]. For $n = 6-9$, the di-anionic E_{gap} is very small and ranges from 0.27 to 0.81 eV, which is narrower than that of corresponding neutral and mono-anionic compounds. The di- and mono-anionic E_{gap} for $n = 10-13, 15,$ and 16 differ little from each other. For $n = 14$, the mono-anionic E_{gap} is smaller than that of the di-anion. The neutral E_{gap} for $n = 10$ and 14 is very close to that of corresponding di-anion. The neutral E_{gap} for $n = 11$ and 16 is larger than that of di-anion. The neutral E_{gap} for $n = 12, 13,$ and 15 is smaller than that of di-anion. The E_{gap} of 2.25 eV for Zintl di-anionic $ZrSi_{15}^{2-}$ is the largest among all these compounds. That is, the Zintl di-anionic $ZrSi_{15}^{2-}$ cluster possesses not only thermodynamic stability, but also chemical stability, which may make it the most suitable building block for novel multi-functional nanomaterials.

2.4. Chemical Bonding Analysis

In order to garner an in-depth comprehension of the ideal chemical and thermodynamic stability of the Zintl di-anionic ZrSi_{15}^{2-} five-capped pentagonal prism, the character of the bonding between the Zr atom and the Si_{15}^{2-} cage is examined by the AdNDP scheme, which is a generalized NBO (Natural Bond Orbital) search strategy to analyze the delocalized and localized multicenter bonds (encoded as $n\text{c-}2\text{e}$, where n can range from 1 (lone pair) to the number of atoms in the cluster) introduced by Zubarev and Boldyrev [35]. As can be seen from Figure 6, the chemical bonding of 66 valence electrons can be split into five types: lone-pair, 2c-2e, 3c-2e, 4c-2e, 10c-2e, and 16c-2e. Each capped Si atom has a lone pair. The pentagonal prism is characterized by ten 2c-2e localized Si-Si σ bonds with 1.86 |e| in each bond. The ten 3c-2e, five 4c-2e, two 10c-2e, and 16c-2e delocalized $\pi+\sigma$ bonds with 1.79–2.00 |e| in each bonds are accountable for the interplay between the inner Zr atom and the outer shell of Si_{15} and enhance the stability of the encapsulated ZrSi_{15}^{2-} molecule.

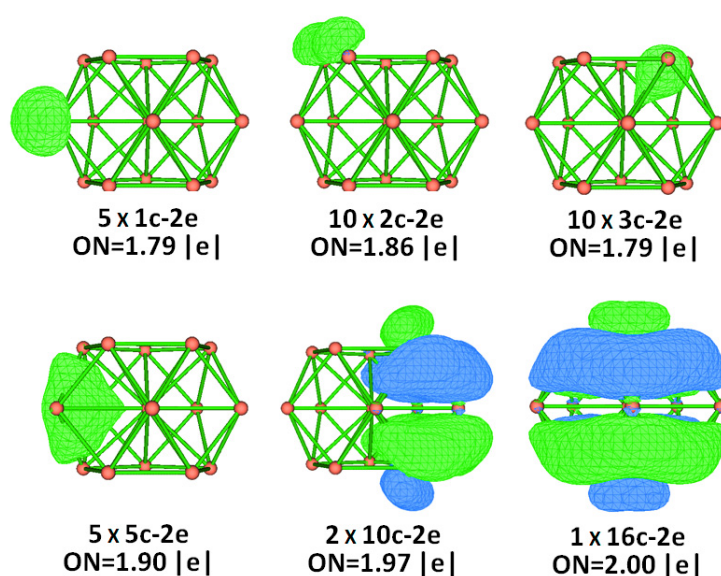


Figure 6. AdNDP analysis of ZrSi_{15}^{2-} cluster. ON stands for the occupation number.

3. Conclusions

The systematic isomer search for low energy structures of neutral, mono-, and di-anionic Zr-doped Si clusters $\text{ZrSi}_n^{0/-2-}$ ($n = 6-16$) are executed by employing an ABCluster global search technique combined with a mPW2PLYP double hybrid density functional scheme. In terms of the evaluated energies, AEA, VDE, and agreement between simulated and experimental PES, the true global minimal structures are confirmed. The results reveal that structural evolution patterns for neutral ZrSi_n clusters prefer the attaching type ($n = 6-9$) to the half-cage motif ($n = 10-13$), and finally to the Zr-encapsulated configuration with the Zr atom centered in a Si cage ($n = 14-16$). For Zintl mono- and di-anionic $\text{ZrSi}_n^{-/2-}$, their growth patterns adopt the attaching configuration ($n = 6-11$) to the encapsulated shape ($n = 12-16$). The calculated AEA for ZrSi_n^- ($n = 6-16$) with the exception of $n = 11, 12$, and 15 are in excellent accord with those of experimental data. The mean absolute deviations from experimental values are 0.08 eV. The further analyses of stability and chemical bonding make it known that two extra electrons not only perfect the structure of ZrSi_{15} but also improve its chemical and thermodynamic stability, which may make it the most suitable building block for novel multi-functional nanomaterials. We think that this study will provide strong motivation for further verification of experimental photoelectron spectroscopy of ZrSi_{11}^- and ZrSi_{15}^- and for further experimental and theoretical studies of other transition metal-doped Si clusters.

4. Theoretical Methods

We utilized three schemes to search the initial isomers of neutral and Zintl anionic $\text{ZrSi}_n^{0/-2-}$ ($n = 6-16$) in order to search for their true global minimum. First, the calculations started from unbiased searches for the low-lying structures of series $\text{ZrSi}_n^{0/-}$ ($n = 6-16$) (with the exception of ZrSi_n^{2-} , of which isomers were chosen in light of ZrSi_n^-) through the ABCluster global search scheme coupled with the GAUSSIAN 09 software suite [36,37]. At least 300 configurations produced by the ABCluster algorithm for each $\text{ZrSi}_n^{0/-}$ ($n = 6-16$) species were optimized at the PBE [38] level with a cc-pVDZ-PP basis set for Zr atoms and a 6-31G basis set for Si atoms [39]. Second, the “substitutional structure”, which is derived from the ground state structure of Si_{n+1} by replacing a Si atom with a Zr atom, was utilized. Third, the structures reported in the preceding publications were utilized [9–18]. Then, the selected low-lying structural candidates were reoptimized at the PBE level with the MIDDLE (cc-pVTZ basis set for Si atoms and basis set for Zr atoms unchanged) basis sets. Vibrational frequency evaluations were also executed at the same level to make sure all the optimized isomers were true local minimum structures. After accomplishment of the preliminary structure optimization through the PBE scheme, the low-lying structural candidates were, again, selected and reoptimized by using the DH-DFT of mPW2PLYP with the MIDDLE basis set [40]. The mPW2PLYP frequency was not calculated. To further refine the energies, single-point energy calculations were finally executed at the mPW2PLYP level with the LARGE (aug-cc-pVTZ basis set for Si atoms and basis set for Zr atoms unchanged) basis set. Moreover, NPA were also executed to further comprehend the interplay between the Zr atom and Si clusters. The PES spectra of the negatively charged ions ZrSi_n^- ($n = 6-16$) were simulated in terms of Koopman’s theorem at the mPW2PLYP/LARGE level via the Multiwfn software suite and compared with the experimental ones [41,42]. The spin multiplicity of singlets, triplets, and quintuplets were considered for neutral ZrSi_n and di-anionic ZrSi_n^{2-} ($n = 6-16$), and doublets and quartets were considered for negatively charged ZrSi_n^- ($n = 6-16$) clusters. To check the reliability of the calculations, the ZrSi structures and properties predicted by mPW2PLYP and CCSD(T) were compared and provided in Table 3. From Table 3 we can see that the order of increasing energy predicted by mPW2PLYP is singlet, to quintet, to the triplet state, which is in agreement with the result evaluated by CCSD(T), while B3LYP is not. On the other hand, the bond dissociation energy (D_0), AEA, and VDE calculated by the mPW2PLYP method were 2.74, 1.44, and 1.45 eV, respectively, which are in good accordance with experimental values of 2.95 [25], 1.46 [24], and 1.58 eV [24]. In particular, the D_0 and AEA predicted by mPW2PLYP among these methods listed in Table 3 is the closest to the experimental data. As a matter of fact, selection of calculation method and basis set is hardly a trivial matter. The cause lies in that the structures and properties predicted by different methods and basis sets may be different. There are many such example. For instance, at the CCSD(T) level, the LanL2DZ basis set for Si atom predicted the ground state of ZrSi was to be triplet state, but 6-311+G(3df,3pd) basis set for Si atom predicted to be singlet state [1].

Table 3. The relative energy of ZrSi between different spin multiplicities along with predicted adiabatic electron affinity (AEA), vertical dissociation energy (VDE), and bond dissociation energy (D_0)^a.

Method	Spin Multiplicity			Property		
	1	3	5	AEA	VDE	D_0
mPW2PLYP/LARGE// mPW2PLYP/MIDDLE	0.00	0.26	0.17	1.44	1.45	2.74
CCSD(T)/LARGE// mPW2PLYP/MIDDLE	0.00	0.26	0.18	1.55	1.56	2.64
B3LYP/LANL2DZ ^b	0.13	0.13	0.00	1.58	1.61	2.51 ^c
B3LYP/mixed basis Set ^b	0.12	0.08	0.00	1.55	1.59	
CCSD(T)/mixed basis set ^b	0.00	0.13	0.10			
Exp.				1.46 ^d	1.58 ^d	2.95 ^c

^a The relative energy, AEA, VDE, and D_0 is in eV. The AEA and VDE were calculated based on the $^2\Sigma^+$ ground state of anionic ZrSi^- ; ^b The data taken from [1]; ^c The data taken from [25]; ^d The data taken from [24].

Supplementary Materials: Supplementary materials can be found at <http://www.mdpi.com/1422-0067/20/12/2933/s1>. Figure S1. Low-lying isomers of neutral $ZrSi_n$ ($n = 6-16$) clusters, point group and relative energy (in eV). Figure S2. Low-lying isomers of mono-anionic $ZrSi_n^-$ ($n = 6-16$) clusters, point group and relative energy (in eV). Figure S3. Low-lying isomers of di-anionic $ZrSi_n^{2-}$ ($n = 6-16$) clusters, point group and relative energy (in eV). Figure S4. The HOMO-LUMO energy gap (E_{gap}) of $ZrSi_n^{0/-/2-}$ ($n = 6-16$) clusters. (m) stands for mPW2PLYP calculations and (p) stands for PBEPBE calculations. Table S1. Conformational population (%) for low-lying geometries of $ZrSi_n^{0/-/2-}$ species ($n = 6-16$) clusters.

Author Contributions: Conceptualization, C.D., L.H.; Formal analysis, C.D., L.H., J.Y.; Writing—original draft, C.D.; Writing—review & editing, C.D., L.H., J.Y., L.C.

Funding: This study was supported by the National Natural Science Foundation of China (grant no. 21863007) and by the Program for Innovative Research Team in the Universities of Inner Mongolia Autonomous Region (grant no. NMGIRT-A1603).

Conflicts of Interest: The authors declare no conflict of interest.

References

1. Gunaratne, K.D.D.; Berkemir, C.; Harmon, C.L.; Castleman, A.W., Jr. Probing the valence orbitals of transition metal-silicon diatomic anions: ZrSi, NbSi, MoSi, PdSi and WSi. *Phys. Chem. Chem. Phys.* **2013**, *15*, 6068–6079. [[CrossRef](#)] [[PubMed](#)]
2. Zhang, S.L.; östling, M. Metal Silicides in CMOS Technology: Past, Present, and Future Trends. *Crit. Rev. Solid State* **2003**, *28*, 1–129. [[CrossRef](#)]
3. Kahng, D.; Lepselter, M.P. Planar Epitaxial Silicon Schottky Barrier Diodes. *Bell Syst. Tech. J.* **1965**, 1525–1527. [[CrossRef](#)]
4. Chen, X.; Jin, J.H.; Sha, G.Y.; Li, C.; Zhang, B.S.; Su, D.S.; Williams, C.T.; Liang, C.H. Silicon-nickel intermetallic compounds supported on silica as a highly efficient catalyst for CO methanation. *Catal. Sci. Technol.* **2014**, *4*, 53–61. [[CrossRef](#)]
5. Zhang, Y.Y.; Zhao, J.; Li, J.H.; Lei, J.; Cheng, X.K. Effect of hot-dip siliconizing time on phase composition and microstructure of Mo-MoSi₂ high temperature structural materials. *Ceram. Int.* **2019**, *45*, 5588–5593. [[CrossRef](#)]
6. Lee, S.J.; Lee, H.Y.; Baik, H.K.; Lee, S.M. Si-Zr alloy thin-film anodes for microbatteries. *J. Power. Sources* **2003**, *119–121*, 113–116. [[CrossRef](#)]
7. Yeom, H.; Jo, H.; Maier, B.; Corradini, M.; Sridharan, K. Multi-Functional Zirconium-Silicide Coatings on Zirconium-alloy for Improved Accident Tolerance. *Trans. Am. Nucl. Soc.* **2017**, *116*, 399–402.
8. Okabayashi, J.; Toyoda, S.; Kumigashira, H.; Oshima, M. Chemical reaction and metallic cluster formation by annealing-temperature control in ZrO₂ gate dielectrics on Si. *Appl. Phys. Lett.* **2004**, *85*, 5959–5961. [[CrossRef](#)]
9. Beck, S.M. Studies of silicon cluster-metal atom compound formation in a supersonic molecular beam. *J. Chem. Phys.* **1987**, *87*, 4233–4234. [[CrossRef](#)]
10. Kumar, V.; Kawazoe, Y. Metal-Encapsulated Fullerenelike and Cubic Caged Clusters of Silicon. *Phys. Rev. Lett.* **2001**, *87*, 045503. [[CrossRef](#)]
11. Kumar, V.; Kawazoe, Y. Magic behavior of Si₁₅M and Si₁₆M (M=Cr, Mo, and W) clusters. *Phys. Rev. B* **2002**, *65*, 073404. [[CrossRef](#)]
12. Kumar, V.; Briere, T.M.; Kawazoe, Y. Ab initio calculations of electronic structures, polarizabilities, Raman and infrared spectra, optical gaps, and absorption spectra of M@Si₁₆ (M=Ti and Zr) clusters. *Phys. Rev. B* **2003**, *68*, 155412. [[CrossRef](#)]
13. Kumar, V.; Majumder, C.; Kawazoe, Y. M@Si₁₆, M = Ti, Zr, Hf: π conjugation, ionization potentials and electron affinities. *Chem. Phys. Lett.* **2002**, *363*, 319–322. [[CrossRef](#)]
14. Kawamura, H.; Kumar, V.; Kawazoe, Y. Growth behavior of metal-doped silicon clusters Si_nM (M=Ti,Zr,Hf; n=8-16). *Phys. Rev. B* **2005**, *71*, 075423. [[CrossRef](#)]
15. Bandyopadhyay, D.; Kumar, M. The electronic structures and properties of transition metal-doped silicon nanoclusters: A density functional investigation. *Chem. Phys.* **2008**, *353*, 170–176. [[CrossRef](#)]
16. Sen, P.; Mitas, L. Electronic structure and ground states of transition metals encapsulated in a Si₁₂ hexagonal prism cage. *Phys. Rev. B* **2003**, *68*, 155404. [[CrossRef](#)]
17. Lu, J.; Nagase, S. Structural and Electronic Properties of Metal-Encapsulated Silicon Clusters in a Large Size Range. *Phys. Rev. Lett.* **2003**, *90*, 115506. [[CrossRef](#)] [[PubMed](#)]

18. Wang, J.; Han, J.G. Geometries, stabilities, and electronic properties of different-sized $ZrSi_n$ ($n = 1-16$) clusters: A density-functional investigation. *J. Chem. Phys.* **2005**, *123*, 064306. [[CrossRef](#)] [[PubMed](#)]
19. Wu, Z.J.; Su, Z.M. Electronic structures and chemical bonding in transition metal monosilicides MSi ($M=3d, 4d, 5d$ elements). *J. Chem. Phys.* **2006**, *124*, 184306. [[CrossRef](#)]
20. Wu, J.H.; Liu, C.X.; Wang, P.; Zhang, S.; Yang, G.; Lu, C. Structures, Stabilities, and Electronic Properties of Small-Sized Zr_2Si_n ($n = 1-11$) Clusters: A Density Functional Study. *Z. Naturforsch.* **2015**, *70*, 805–814. [[CrossRef](#)]
21. Wang, J.; Liu, J.H. Investigation of Size-Selective $Zr_2@Si_n$ ($n = 16-24$) Caged Clusters. *J. Phys. Chem. A* **2008**, *114*, 4562–4567. [[CrossRef](#)] [[PubMed](#)]
22. Koyasu, K.; Atobe, J.; Akutsu, M.; Mitsui, M.; Nakajima, A. Electronic and Geometric Stabilities of Clusters with Transition Metal Encapsulated by Silicon. *J. Phys. Chem. A* **2007**, *111*, 42–49. [[CrossRef](#)] [[PubMed](#)]
23. Koyasu, K.; Atobe, J.; Furuse, S.; Nakajima, A. Anion photoelectron spectroscopy of transition metal- and lanthanide metal-silicon clusters: MSi_n^- ($n = 6-20$). *J. Chem. Phys.* **2008**, *129*, 214301. [[CrossRef](#)] [[PubMed](#)]
24. Gunaratne, K.D.D.; Hazra, A.; Castleman, A.W., Jr. Photoelectron imaging spectroscopy and theoretical investigation of $ZrSi$. *J. Chem. Phys.* **2011**, *134*, 204303. [[CrossRef](#)] [[PubMed](#)]
25. Sevy, A.; Sorensen, J.J.; Persinger, T.D.; Franchina, J.A. Bond dissociation energies of $TiSi$, $ZrSi$, $HfSi$, VSi , $NbSi$, and $TaSi$. *J. Chem. Phys.* **2017**, *147*, 084301. [[CrossRef](#)] [[PubMed](#)]
26. Maroulis, G.; Begué, D.; Pouchan, C. Accurate dipole polarizabilities of small silicon clusters from ab initio and density functional theory calculations. *J. Chem. Phys.* **2003**, *119*, 794–797. [[CrossRef](#)]
27. Maroulis, G. Quantifying the Performance of Conventional DFT Methods on a Class of Difficult Problems: The Interaction (Hyper)Polarizability of Two Water Molecules as a Test Case. *Int. J. Quantum Chem.* **2012**, *112*, 2231–2241. [[CrossRef](#)]
28. Jiang, W.Y.; Laury, M.L.; Powell, M.; Wilson, A.K. Comparative Study of Single and Double Hybrid Density Functionals for the Prediction of 3d Transition Metal Thermochemistry. *J. Chem. Theory Comput.* **2012**, *8*, 4102–4111. [[CrossRef](#)]
29. Liu, Y.M.; Yang, J.C.; Cheng, L. Structural Stability and Evolution of Scandium-Doped Silicon Clusters: Evolution of Linked to Encapsulated Structures and Its Influence on the Prediction of Electron Affinities for $ScSi_n$ ($n = 4-16$) Clusters. *Inorg. Chem.* **2018**, *57*, 12934–12940. [[CrossRef](#)]
30. Chen, B.L.; Sun, W.G.; Kuang, X.Y.; Lu, C.; Xia, X.X.; Shi, H.X.; Maroulis, G. Structural Stability and Evolution of Medium-Sized Tantalum-Doped Boron Clusters: A Half-Sandwich-Structured TaB_{12}^- Cluster. *Inorg. Chem.* **2018**, *57*, 343–350. [[CrossRef](#)]
31. Xing, X.D.; Hermann, A.; Kuang, X.Y.; Ju, M.; Lu, C.; Jin, Y.Y.; Xia, X.X.; Maroulis, G. Insights into the geometries, electronic and magnetic properties of neutral and charged palladium clusters. *Sci. Rep.* **2016**, *6*, 19656. [[CrossRef](#)] [[PubMed](#)]
32. Jin, Y.Y.; Maroulis, G.; Kuang, X.Y.; Ding, L.P.; Lu, C.; Wang, J.J.; Lv, J.; Zhang, C.Z.; Ju, M. Geometries, stabilities and fragmental channels of neutral and charged sulfur clusters: S_n^Q ($n = 3-20$, $Q = 0, \pm 1$). *Phys. Chem. Chem. Phys.* **2015**, *17*, 13590–13597. [[CrossRef](#)] [[PubMed](#)]
33. Wu, X.; Zhou, S.; Huang, X.M.; Chen, M.; King, R.B.; Zhao, J.J. Revisit of Large-Gap Si_{16} Clusters Encapsulating Group-IV Metal Atoms (Ti, Zr, Hf). *J. Comput. Chem.* **2018**, *39*, 2268–2272. [[CrossRef](#)] [[PubMed](#)]
34. Baerends, E.J.; Gritsenko, O.V.; Meer, R.V. The Kohn-Sham gap, the fundamental gap and the optical gap: the physical meaning of occupied and virtual Kohn-Sham orbital energies. *Phys. Chem. Chem. Phys.* **2013**, *15*, 16408–16425. [[CrossRef](#)] [[PubMed](#)]
35. Zubarev, D.Y.; Boldyrev, A.I. Developing paradigms of chemical bonding: adaptive natural density partitioning. *Phys. Chem. Chem. Phys.* **2008**, *10*, 5207–5217. [[CrossRef](#)] [[PubMed](#)]
36. Zhang, J.; Dolg, M. ABCluster: the artificial bee colony algorithm for cluster global optimization. *Phys. Chem. Chem. Phys.* **2015**, *17*, 24173–24181. [[CrossRef](#)] [[PubMed](#)]
37. Frisch, M.J.; Trucks, G.W.; Schlegel, H.B.; Scuseria, G.E.; Robb, M.A.; Cheeseman, J.R.; Scalmani, G.; Barone, V.; Mennucci, B.; Petersson, G.A.; et al. *Gaussian09, Revision, C.01*; Gaussian, Inc.: Wallingford, CT, USA, 2010.
38. Perdew, J.P.; Burke, K.; Ernzerhof, M. Generalized Gradient Approximation Made Simple. *Phys. Rev. Lett.* **1996**, *77*, 3865–3868. [[CrossRef](#)]
39. Peterson, K.A.; Figgen, D.; Dolg, M.; Stoll, H. Energy-consistent relativistic pseudopotentials and correlation consistent basis sets for the 4d elements Y-Pd. *J. Chem. Phys.* **2007**, *126*, 124101. [[CrossRef](#)]

40. Schwabe, T.; Grimme, S. Towards chemical accuracy for the thermodynamics of large molecules: new hybrid density functionals including non-local correlation effects. *Phys. Chem. Chem. Phys.* **2006**, *8*, 4398–4401. [[CrossRef](#)]
41. Akola, J.; Manninen, M.; Häkkinen, H.; Landman, U.; Li, X.; Wang, L.S. Photoelectron spectra of aluminum cluster anions: Temperature effects and ab initio simulations. *Phys. Rev. B* **1999**, *60*, R11297–R11300. [[CrossRef](#)]
42. Lu, T.; Chen, F.W. Multiwfn: A Multifunctional Wavefunction Analyzer. *J. Comput. Chem.* **2012**, *33*, 580–592. [[CrossRef](#)] [[PubMed](#)]



© 2019 by the authors. Licensee MDPI, Basel, Switzerland. This article is an open access article distributed under the terms and conditions of the Creative Commons Attribution (CC BY) license (<http://creativecommons.org/licenses/by/4.0/>).